Electronic Supplementary Information

Excess axial electrostatic repulsion as a criterion for pentagonal bipyramidal Dy^{III} single-ion magnets with high U_{eff} and T_B

Zhijie Jiang,[‡] Lin Sun,[‡] Qi Yang, Bing Yin,[*] Hongshan Ke, Jing Han, Qing Wei, Gang Xie, and Sanping Chen[*]

Key Laboratory of Synthetic and Natural Functional Molecule Chemistry of Ministry of Education, College of Chemistry and Materials Science, Northwest University, Xi'an, Shaanxi 710127, China.

Corresponding authors

Prof. Sanping Chen, Prof. Bing Yin

E-mail address: sanpingchen@126.com; rayinyin@nwu.edu.cn**;**

Table of Contents

1. X-ray crystallographic data

Table S1. Crystal data and structure refinement for complexes **1** and **2**.

Complex	**1**	**2**
Empirical formula	$C_{30}H_{32}ClDyN_4O_2$	$C_{30}H_{32}BrDyN_4O_2$
Formula weight	678.55	723.01
Crystal system	Monoclinic	Monoclinic
Space group	$P2_1/n$	$P2_1/n$
a(Å)	8.6164(9)	8.606(3)
b(Å)	18.5966(19)	18.545(6)
c(Å)	17.2232(17)	17.441(6)
α(°)	90.00	90.00
β(°)	92.760(2)	93.068(5)
γ(°)	90.00	90.00
V(Å3)	2756.6(5)	2779.5(15)
Z	4	4
F(000)	1356	1428
$R1^{[a]}$, [I > 2σ(I)]	0.0285	0.0565
w$R_2^{[b]}$, [I > 2σ(I)]	0.0609	0.1644
$R1^a$, (all data)	0.0402	0.0623
wR_2^b, (all data)	0.0707	0.1687
GOF on F^2	1.045	1.031

$^aR_1 = \Sigma(F_o - F_c)/\Sigma F_o$. $^bwR_2 = [\Sigma w(F_o^2 - F_c^2)^2/\Sigma w(F_o^2)^2]^{1/2a}$.

Table S2. Selected bond lengths and angles for complexes **1** and **2**.

1					
Dy(1)-O(1)	2.155(3)	O(1)-Dy(1)-N(5)	97.44(12)	N(5)-Dy(1)-N(4)	64.52(11)
Dy(1)-O(2)	2.166(3)	O(2)-Dy(1)-N(5)	87.65(11)	N(2)-Dy(1)-N(4)	69.02(11)
Dy(1)-N(1)	2.568(4)	N(1)-Dy(1)-N(5)	161.92(12)	O(1)-Dy(1)-Cl(1)	101.52(8)
Dy(1)-N(5)	2.589(4)	O(1)-Dy(1)-N(2)	83.89(11)	O(2)-Dy(1)-Cl(1)	100.33(8)
Dy(1)-N(2)	2.601(3)	O(2)-Dy(1)-N(2)	76.94(11)	N(1)-Dy(1)-Cl(1)	81.38(9)
Dy(1)-N(4)	2.606(3)	N(1)-Dy(1)-N(2)	65.24(11)	N(5)-Dy(1)-Cl(1)	81.06(9)
Dy(1)-Cl(1)	2.6580(12)	N(5)-Dy(1)-N(2)	131.69(11)	N(2)-Dy(1)-Cl(1)	146.30(8)
O(1)-Dy(1)-O(2)	158.07(11)	O(1)-Dy(1)-N(4)	76.62(11)	N(4)-Dy(1)-Cl(1)	144.68(8)
O(1)-Dy(1)-N(1)	90.23(11)	O(2)-Dy(1)-N(4)	86.55(11)		
O(2)-Dy(1)-N(1)	91.31(12)	N(1)-Dy(1)-N(4)	133.45(11)		

2					
Dy(1)-O(1)	2.141(6)	O(1)-Dy(1)-N(3)	87.5(2)	N(3)-Dy(1)-N(4)	65.1(2)
Dy(1)-O(2)	2.151(7)	O(2)-Dy(1)-N(3)	76.8(2)	N(1)-Dy(1)-N(4)	132.6(2)
Dy(1)-N(2)	2.567(8)	N(2)-Dy(1)-N(3)	133.6(2)	O(1)-Dy(1)-Br(1)	99.26(16)
Dy(1)-N(3)	2.582(7)	O(1)-Dy(1)-N(1)	77.5(2)	O(2)-Dy(1)-Br(1)	101.26(17)
Dy(1)-N(1)	2.590(7)	O(2)-Dy(1)-N(1)	84.3(2)	N(2)-Dy(1)-Br(1)	81.47(18)
Dy(1)-N(4)	2.603(8)	N(2)-Dy(1)-N(1)	65.3(2)	N(3)-Dy(1)-Br(1)	144.44(17)
Dy(1)-Br(1)	2.8356(14)	N(3)-Dy(1)-N(1)	69.1(2)	N(1)-Dy(1)-Br(1)	146.41(18)
O(1)-Dy(1)-O(2)	159.4(2)	O(1)-Dy(1)-N(4)	88.7(3)	N(4)-Dy(1)-Br(1)	80.10(17)
O(1)-Dy(1)-N(2)	90.8(3)	O(2)-Dy(1)-N(4)	96.7(3)		
O(2)-Dy(1)-N(2)	90.4(3)	N(2)-Dy(1)-N(4)	161.2(2)		

Table S3. The calculated results for Dy^{III} ions configuration of complexes **1** and **2** by SHAPE 2.1 software.

Configuration	ABOXIY, **1**	ABOXIY, **2**
Heptagon (D_{7h})	33.230	33.143
Hexagonal pyramid (C_{6v})	23.340	23.452
Pentagonal bipyramid (D_{5h})	**1.824**	**2.111**
Capped octahedron (C_{3v})	7.899	8.343
Capped trigonal prism (C_{2v})	6.102	6.461
Johnson pentagonal bipyramid J13 (D_{5h})	2.209	2.235
Johnson elongated triangular pyramid J7 (C_{3v})	21.882	22.465

Table S4. Deviations (Å) from the ideal plane defined by five coordination atoms for complexes **1**, **1′** , **2**, **2′** and **3**. The positive value denotes that the atom is located on the same side of the Dy atom, whereas a negative value denotes that the atom is located on the opposite side.

Complex	**Coordination atoms**					**r.m.s. deviation**
3	0.0995	-0.1170	0.0903	-0.0265	-0.0477	0.0833
2	-0.0046	-0.0528	0.1548	-0.2179	0.1837	0.1468
2′	0.1204	0.2111	-0.2111	-0.1204	0.0000	0.1536
1	-0.1632	0.2343	-0.1887	0.0194	0.0402	0.1543
1′	0.2239	-0.1292	0.1292	-0.2239	0.0000	0.1634

Table S5. The distances between neighboring molecules packing along *a*, *b* and *c* directions for complexes **1** and **2**.

Direction of Dy⋯Dy	**Complex 1**	**Complex 2**

along *a* direction	8.6164	8.6060
along *b* direction	8.4789	8.4697
along *c* direction	9.4825	9.5535

2. The ^{1}H NMR spectra of H_2bbpen-CH_3

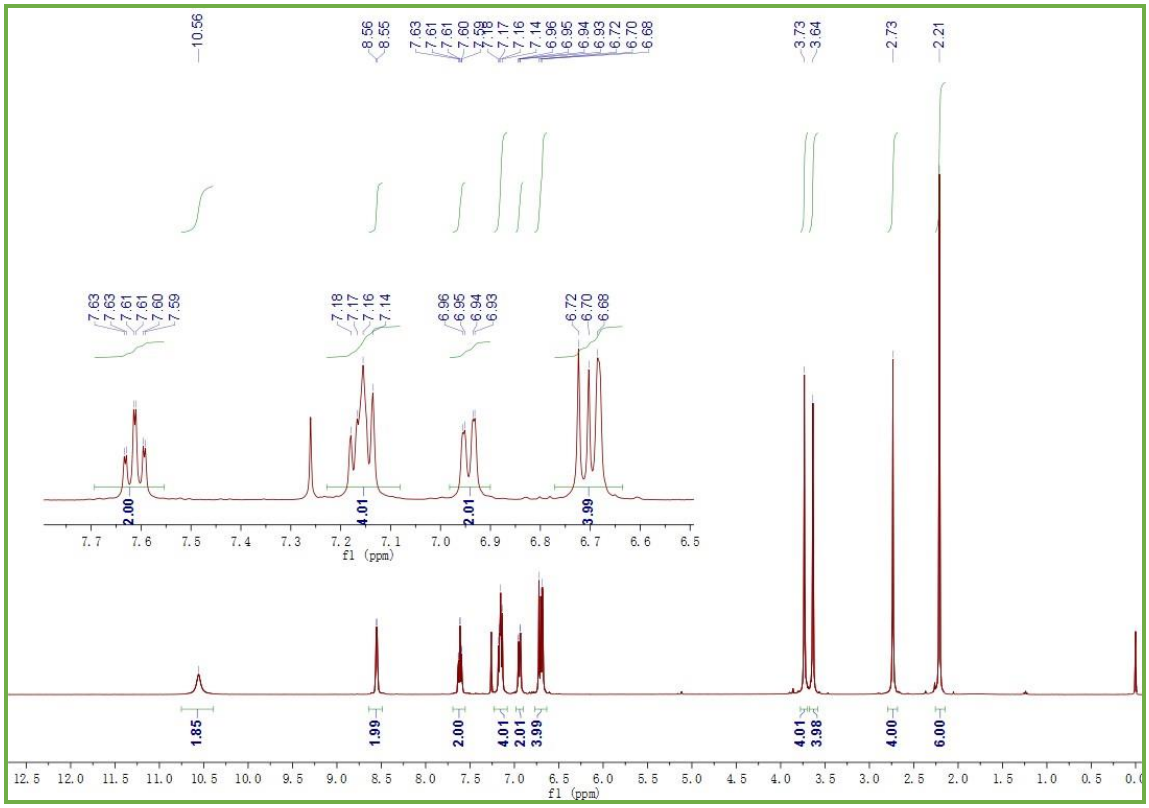

Figure S1. ^{1}H-NMR spectra of the ligand H_2bbpen-CH_3.

3. X-Ray Powder Diffraction

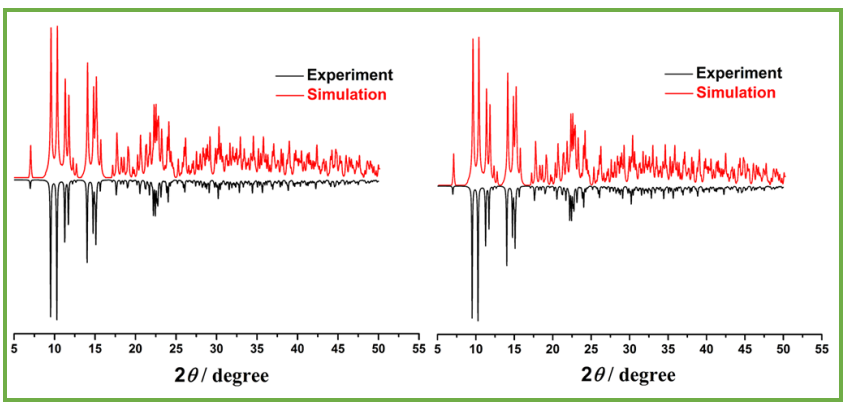

Figure S2. Experimental and simulated PXRD of complexes **1** (left) and **2** (right).

4. Crystal Structure

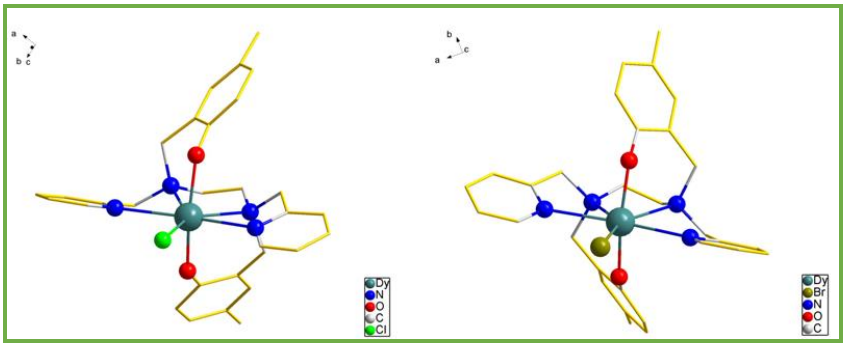

Figure S3. Molecular structures for **1** (left) and **2** (right). Hydrogen atoms are omitted for clarity. Color codes: Dy, blackish green; Cl, green; Br, brown; O, red; N, blue; C, silver.

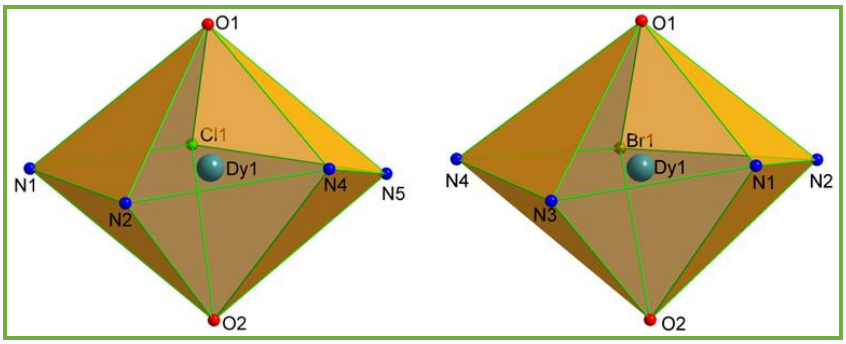

Figure S4. Polyhedrons showing D_{5h} symmetry around Dy^{III} ion for **1** (left) and **2** (right).

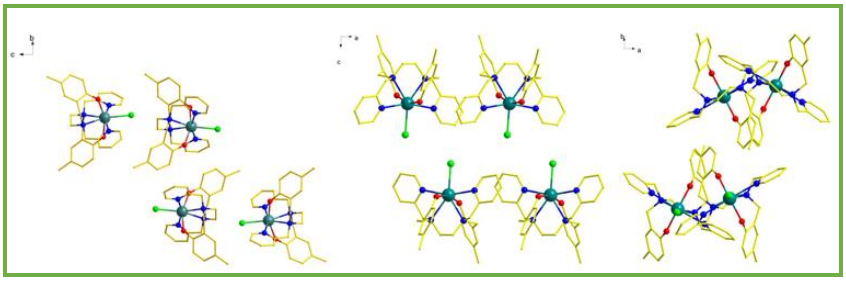

Figure S5. Packing diagram for complex **1** along *a*, *b*, *c* axises (from left to right).

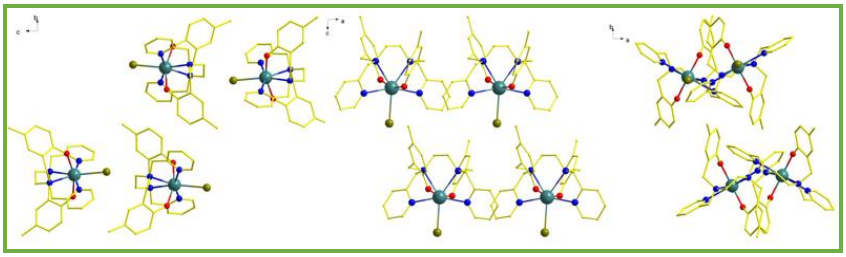

Figure S6. Packing diagram for complex **2** along *a*, *b*, *c* axises (from left to right).

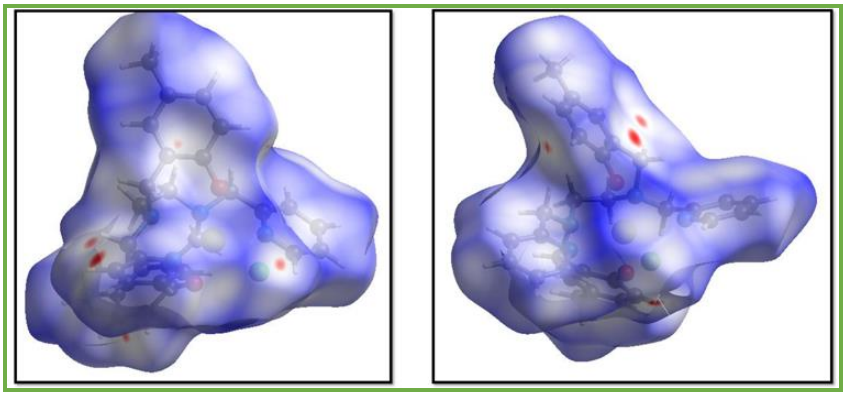

Figure S7. Hirshfeld surfaces calculation of complexes **1** (left) and **2** (right).

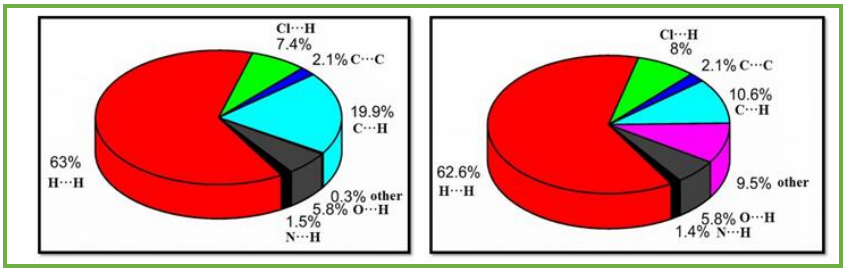

Figure S8. The individual atomic contact percentage contribution to the Hirshfeld surface for complexes **1** (left) and **2** (right).

5. Magnetic Measurements

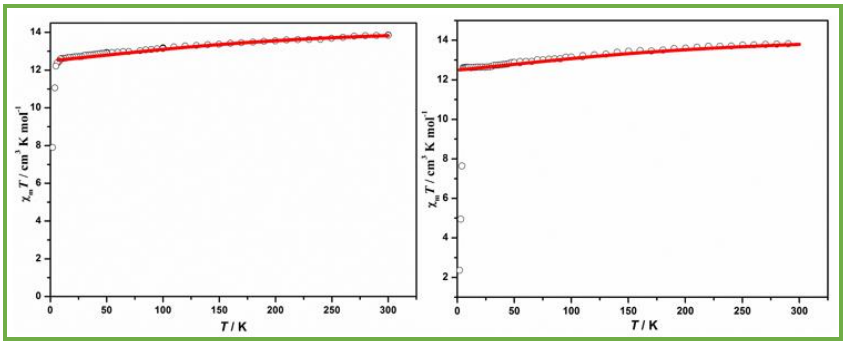

Figure S9. Field-dependencies of magnetization for complexes **1** (left) and **2** (right) at indicated temperatures. The field range is 0-7 T. The solid lines correspond to the *ab initio* calculations.

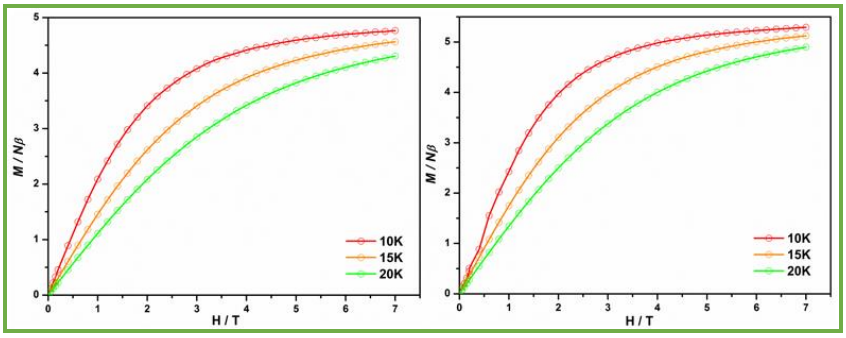

Figure S10. Variable field magnetisation of complexes **1** and **2**, at temperatures of 10 K, 15 K and 20 K.

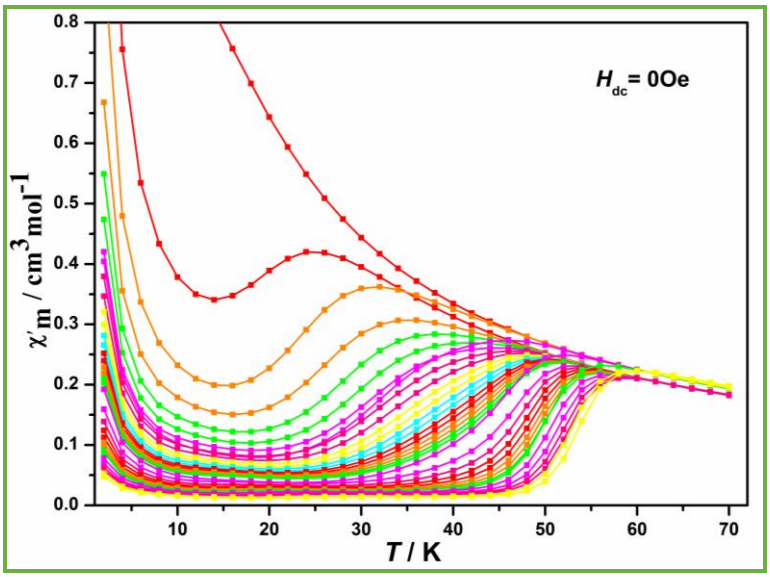

Figure S11. Temperature dependence of the in-phase in zero dc field for complex **1**.

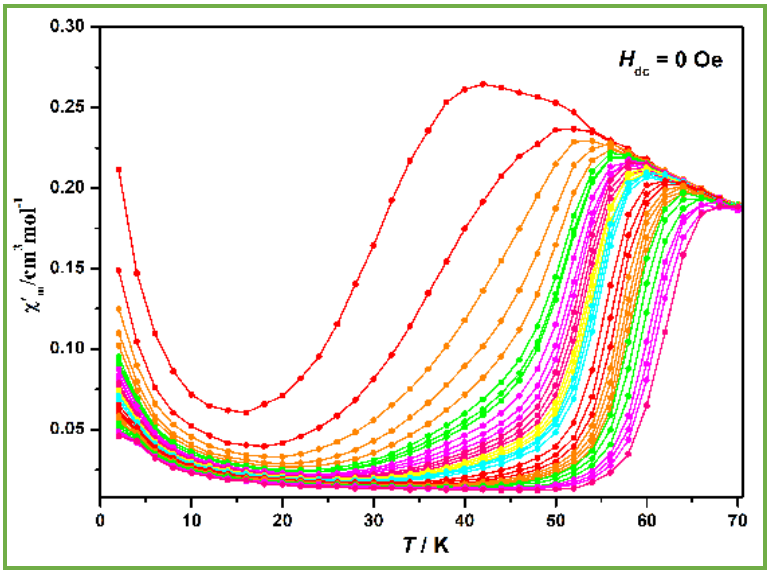

Figure S12. Temperature dependence of the in-phase in zero dc field for complex **2**.

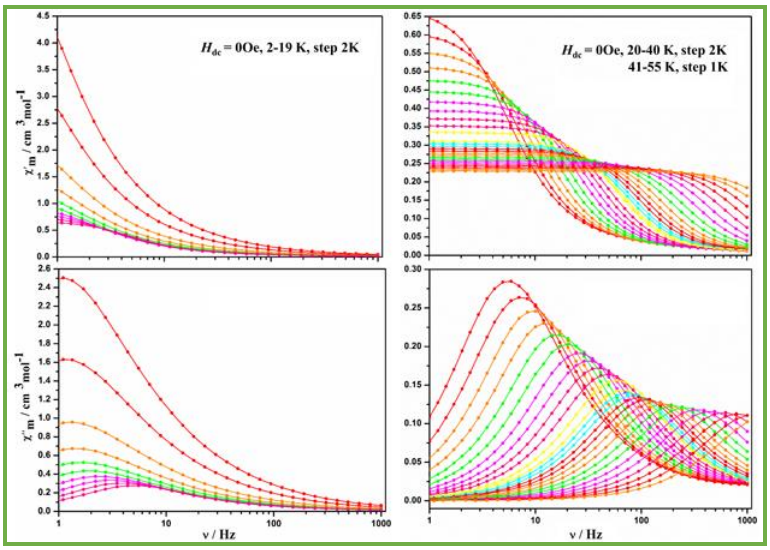

Figure S13. Variable frequency in-phase (top) and out-of-phase (bottom) magnetic susceptibility in zero dc field for complex **1** with the ac frequency of 1-1000 Hz.

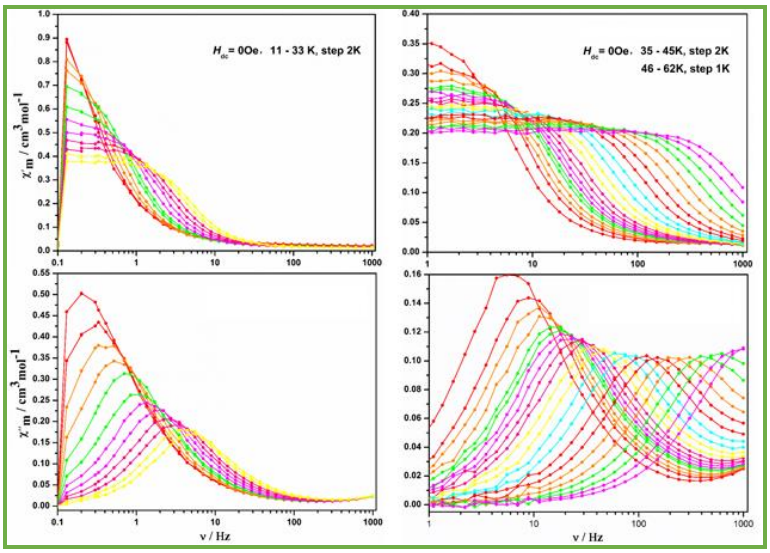

Figure S14. Variable frequency in-phase (top) and out-of-phase (bottom) magnetic susceptibility in zero dc field for complex **2** with the ac frequency of 1-1000 Hz.

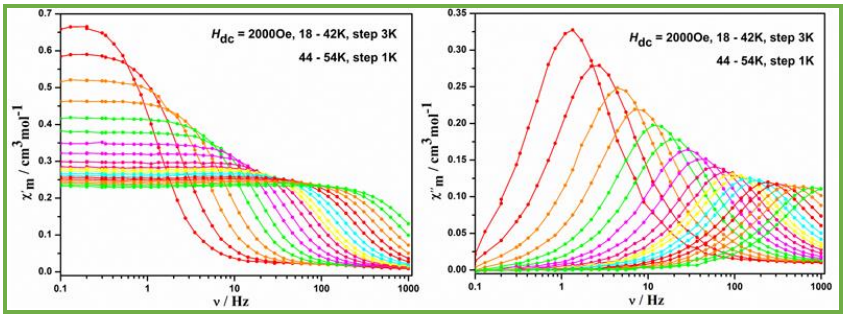

Figure S15. Variable frequency in-phase (χ_m') (left) and (right) out-of-phase (χ_m'') components of the ac magnetic susceptibility for complex **1** between 18 and 54 K under 2000 Oe applied dc field.

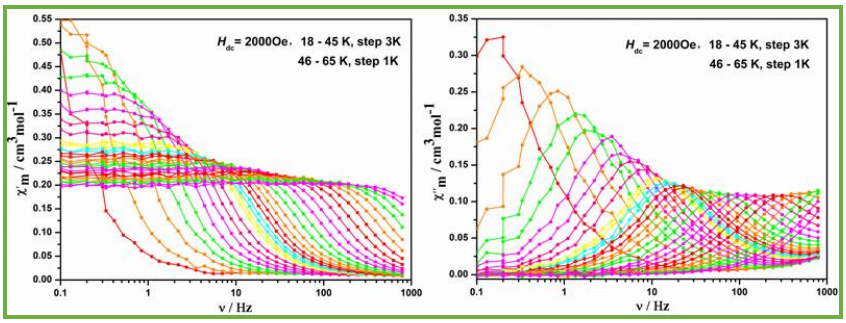

Figure S16. Variable frequency in-phase (χ_m') (left) and (right) out-of-phase (χ_m'') components of the ac magnetic susceptibility for complex **2** between 18 and 65 K under 2000 Oe applied dc field.

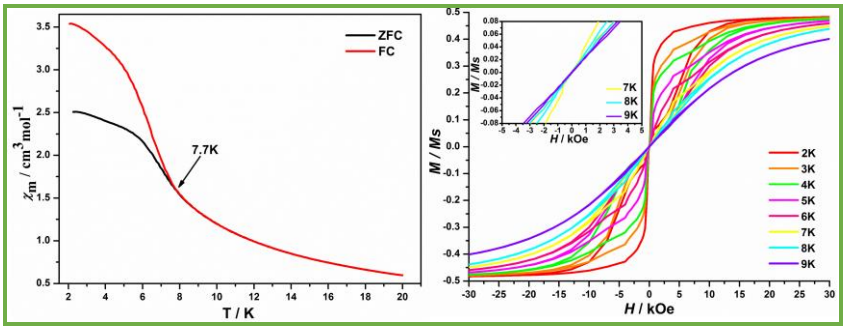

Figure S17. Variable-field magnetization data for complex **1**, under field-cooled (FC) and zero-field-cooled (ZFC) conditions with a field of 2000 Oe (left). Magnetic hysteresis loops were measured at a sweep rate of 0.02 T s-1 from 2 to 9 K (right).

6. Fitting for complexes 1 and 2

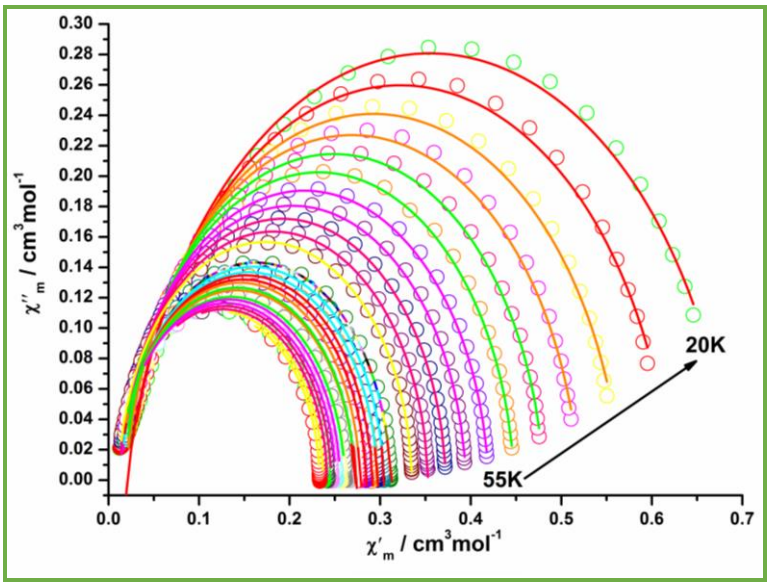

Figure S18. Cole-Cole plot for complex **1**. The solid lines are the best fits for the generalized Debye model between 20 K and 55 K.

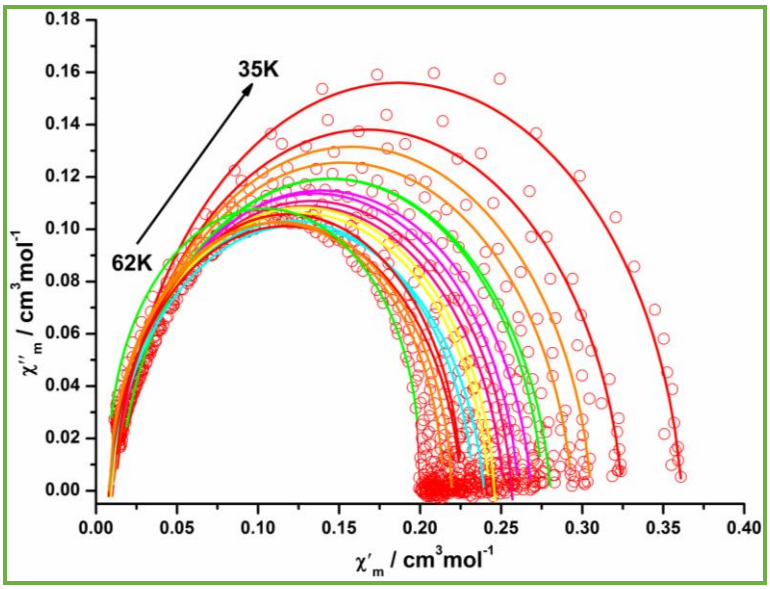

Figure S19. Cole-Cole plot for complex **2**. The solid lines are the best fits for the generalized Debye model between 35 K and 62 K.

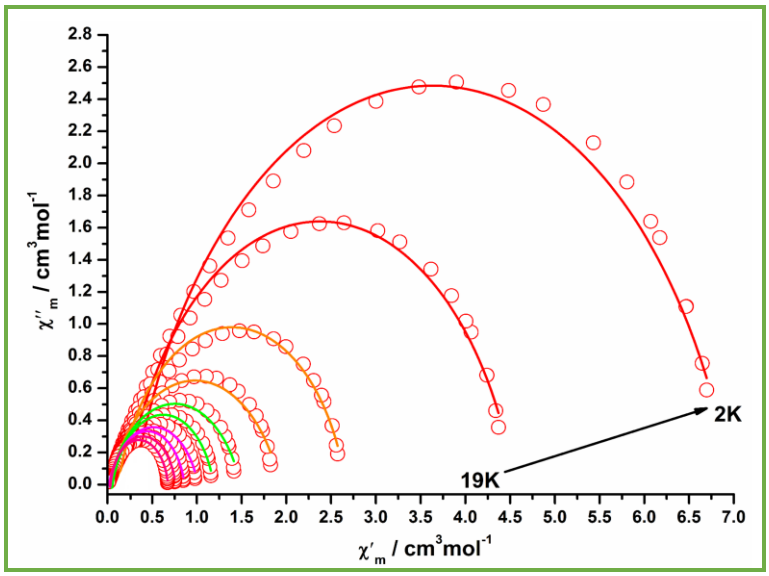

Figure S20. Cole-Cole plot of complex **1**. The solid lines are the best fits for the generalized Debye model between 2 K and 19 K.

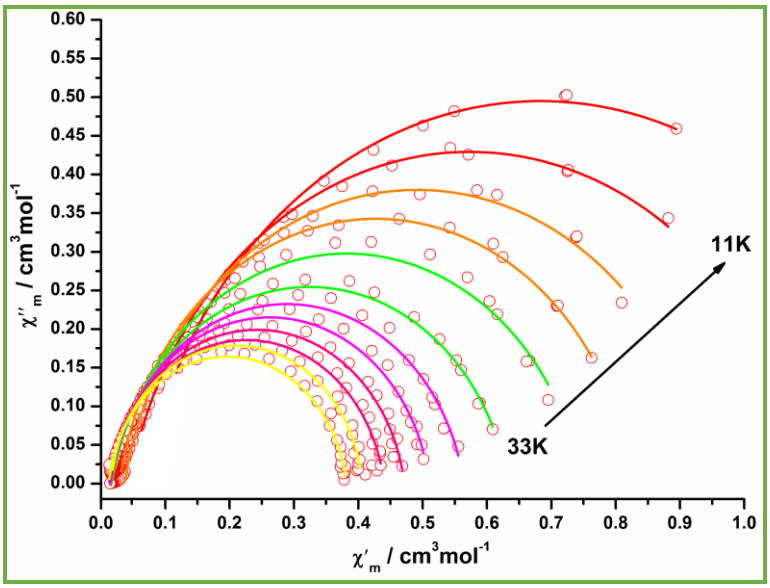

Figure S21. Cole-Cole plot of complex **2**. The solid lines are the best fits for the generalized Debye model between 11K and 33 K.

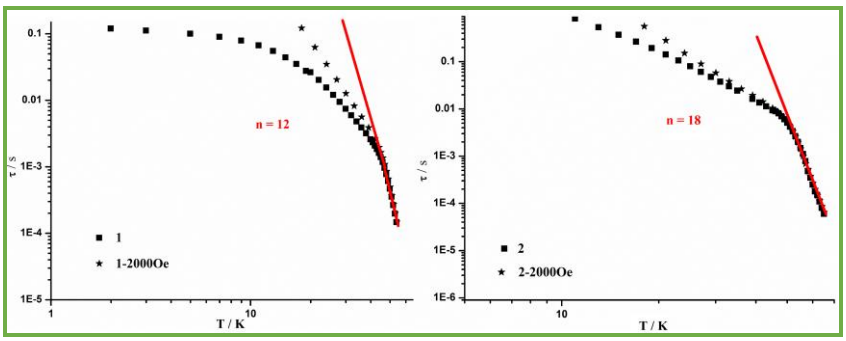

Figure S22. Temperature dependences of the magnetic relaxation times (τ) in log-log scale for

complexes **1** and **2**.

7. Computational details

Table S6. *Ab initio* computed relatives energies (cm^{-1}), principal values of the *g*-tensors and averaged transition magnetic moment μ_{QTM} (in μ_B) of the eight lowest KDs of the complexes **1′** , **1**, **2′** , **2** and **3**.

		1′	**1**	**2′**	**2**	**3**
KD_0	*E*	0.000	0.000	0.000	0.000	0.000
	g_Z	**19.87402**	**19.87766**	**19.87993**	**19.88260**	**19.88907**
	g_X	0.12483×10^{-2}	0.91759×10^{-3}	0.53783×10^{-3}	0.24718×10^{-3}	0.29090×10^{-5}
	g_Y	0.16190×10^{-2}	0.12864×10^{-2}	0.64102×10^{-3}	0.36162×10^{-3}	0.42090×10^{-5}
	g_{XY}	0.20443×10^{-2}	0.15801×10^{-2}	0.83676×10^{-3}	0.43802×10^{-3}	0.51164×10^{-5}
	g_{XY}/g_Z	$\mathbf{0.10286\times10^{-3}}$	$\mathbf{0.79492\times10^{-4}}$	$\mathbf{0.42091\times10^{-4}}$	$\mathbf{0.22030\times10^{-4}}$	$\mathbf{0.25725\times10^{-6}}$
	μ_{QTM}	$\mathbf{0.47788\times10^{-3}}$	$\mathbf{0.36733\times10^{-3}}$	$\mathbf{0.19647\times10^{-3}}$	$\mathbf{0.10147\times10^{-3}}$	$\mathbf{0.11863\times10^{-5}}$
KD_1	*E*	371.009	399.370	390.437	422.389	559.490
	g_Z	16.89390	16.95598	16.98390	17.00573	16.96779
	g_X	0.12821	0.99731×10^{-1}	0.68103×10^{-1}	0.54774×10^{-1}	0.42950×10^{-3}
	g_Y	0.19389	0.13304	0.85862×10^{-1}	0.62064×10^{-1}	0.46806×10^{-3}
	g_{XY}	0.23244	0.16627	0.10959	0.82777	0.63525×10^{-3}
	g_{XY}/g_Z	0.13759×10^{-1}	0.98062×10^{-2}	0.64527×10^{-2}	0.48676×10^{-2}	0.37439×10^{-4}
	μ_{QTM}	0.53683×10^{-1}	0.38795×10^{-2}	0.25661×10^{-2}	0.19473×10^{-2}	0.14959×10^{-3}
	θ	0.55	1.76	0.52	2.11	0.40
KD_2	*E*	558.785	634.225	618.449	694.441	930.513
	g_Z	10.77129	12.37989	13.50033	13.90615	14.27792
	g_X	0.25243×10	0.18065×10	0.84548	0.47723	0.44008×10^{-1}
	g_Y	0.63962×10	0.37776×10	0.15364×10	0.79635	0.47497×10^{-1}
	g_{XY}	0.68763×10	0.41873×10	0.17537×10	0.92839	0.64751×10^{-1}
	g_{XY}/g_Z	0.63839	0.33824	0.12990	0.66761×10^{-1}	0.45350×10^{-2}
	μ_{QTM}	0.14868×10	0.93068	0.39698	0.21226	0.15251×10^{-1}
	θ	0.60000	5.30000	0.09000	5.30000	1.60000
KD_3	*E*	622.856	717.516	708.647	819.567	1126.031
	g_Z	1.54149	10.19307	9.71060	9.25238	11.00216
	g_X	0.72451×10	0.20641×10	0.48217×10	0.45147×10	0.51882
	g_Y	0.60805×10	0.58435×10	0.61028×10	0.57474×10	0.93728
	g_{XY}	0.94586×10	0.61973×10	0.77778×10	0.73086×10	0.10713×10
	g_{XY}/g_Z	0.61360×10	0.60800	0.80096	0.78991	0.97371×10^{-1}
	μ_{QTM}	0.22209×10	0.13179×10	0.18208×10	0.17104×10	0.24268
	θ	12.48000	84.68000	90.00000	74.07000	5.90000

KD_4	*E*	691.048	791.705	765.468	863.391	1155.752
	g_Z	11.32019	11.05055	10.49331	10.09497	16.81698
	g_X	0.12969×10	0.48518	0.34816	0.14547×10	0.54409×10^{-1}
	g_Y	0.19106×10	0.46627×10	0.42690×10	0.48303×10	0.19843×10
	g_{XY}	0.23092×10	0.46879E×10	0.42832×10	0.50446×10	0.19850×10
	g_{XY}/g_Z	0.20399	0.42422	0.40818	0.49972	0.11804
	μ_{QTM}	0.53458	0.85798	0.76953	0.10475×10	0.33978
	θ	74.90000	95.91000	72.22000	93.19000	88.12000
KD_5	E	713.275	805.464	778.095	877.336	1191.531
	g_Z	13.95325	11.92035	15.57009	9.06478	2.76496
	g_X	0.35431×10^{-1}	0.11612×10	0.18543	0.89482	0.95601×10
	g_Y	0.33793	0.39939×10	0.15844×10	0.47383×10	0.81047×10
	g_{XY}	0.33978	0.41593×10	0.15952×10	0.48220×10	0.12533×10^{2}
	g_{XY}/g_Z	0.24352×10^{-1}	0.34893	0.10245	0.53195	0.45329×10
	μ_{QTM}	0.62227×10^{-1}	0.85918	0.29497	0.93885	0.29441×10
	θ	97.56000	96.82000	85.56000	86.13000	12.74000
KD_6	E	730.748	826.973	784.950	897.785	1210.806
	g_Z	18.25953	16.63400	12.27662	10.06968	15.00569
	g_X	0.97817×10^{-1}	0.99311×10^{-1}	0.15556×10	0.12124	0.13508×10
	g_Y	0.13030	0.10948×10	0.31525×10	0.28780×10	0.31727×10
	g_{XY}	0.16293	0.10993×10	0.35154×10	0.28806×10	0.34483×10
	g_{XY}/g_Z	0.89230×10^{-2}	0.66086×10^{-1}	0.28635	0.28607	0.22980
	μ_{QTM}	0.38019×10^{-1}	0.19902	0.78468	0.49987	0.75392
	θ	75.69000	92.23000	84.93000	92.43000	87.89000
KD_7	*E*	809.347	873.100	853.009	944.216	1224.079
	g_Z	19.04282	16.86389	18.23157	15.41390	13.67243
	g_X	0.14486×10^{-1}	0.53676	0.17011	0.10363×10	0.39835
	g_Y	0.52539×10^{-1}	0.86355	0.25651	0.32077×10	0.59629×10
	g_{XY}	0.54499×10^{-1}	0.10168×10	0.30779	0.33710×10	0.59762×10
	g_{XY}/g_Z	0.28619×10^{-2}	0.60293×10^{-1}	0.16882×10^{-1}	0.21870	0.43710
	μ_{QTM}	0.11171×10^{-1}	0.23339	0.71103×10^{-1}	0.70733	0.10602×10
	θ	109.05000	91.67000	107.82000	104.69000	88.75000

[a] Theoretical results calculated on structures including one solvent molecule are shown in parentheses.

Table S7. The angle between the *ab initio* easy axis and the axial Dy-O bond of complexes **1** and **2**.

Complex	θ1(O2)	θ2(O3)	averaged
1	10.764	11.192	10.978
2	10.448	10.196	10.322

[a] deviation from the magnetic hard plane. [b] deviation from the averaged Z coordinate.

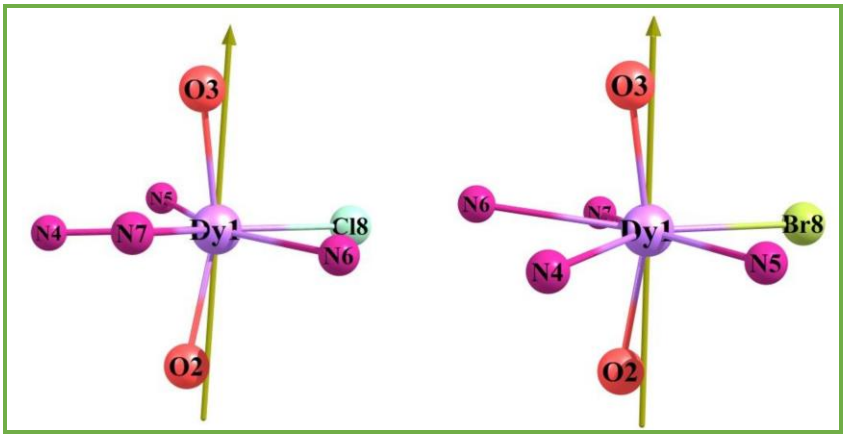

Figure S23. Direction of the *ab initio* magnetic easy axis of ground KD of complexes **1** and **2** (only central Dy^{III} and first sphere are shown for the sake of clarity).

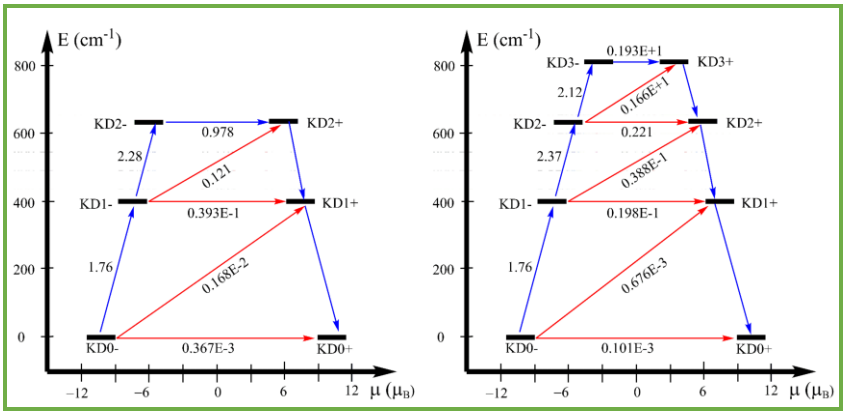

Figure S24. Magnetization blocking barrier in **1** (left) and **2** (right). Exchange states are arranged according to the values of their magnetic moments (bold horizontal black lines). Arrows show the transition between the states, while the numbers above the arrows are the corresponding average matrix element of the magnetic moment (μ). Relaxation pathway is outlined by arrows containing the largest μ (blue arrows).

8. Discussion section

Table S8. U_{eff} and T_B for complexes **1′** , **1**, **2′** , **2** and **3**.

Complex	**1′**	**1**	**2′**	**2**	**3**
U_{eff} **/K**	708	723	1025	1162	1837
T_B **(0.02 T·s^{-1})**	8	9	14	15	-

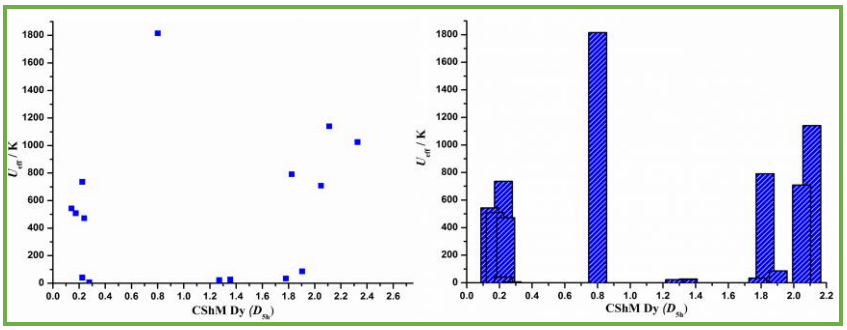

Figure S25. CshM *vs* U_{eff} for some typical D_{5h} Dy^{III}-SMM.

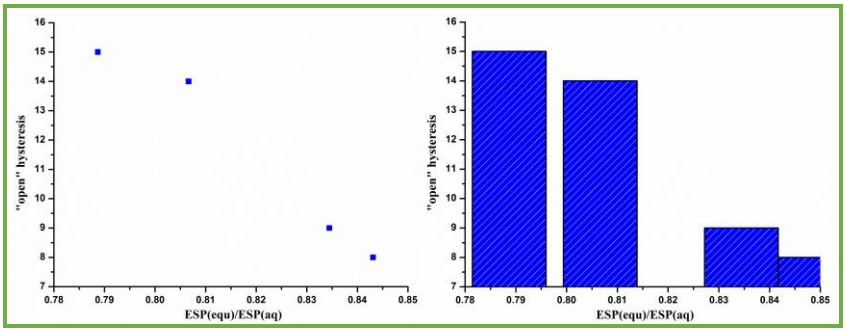

Figure S26. ESP(equ)/ESP(ax) *vs* "open" hysteresis for complexes **1′** , **1**, **2′** and **2**.

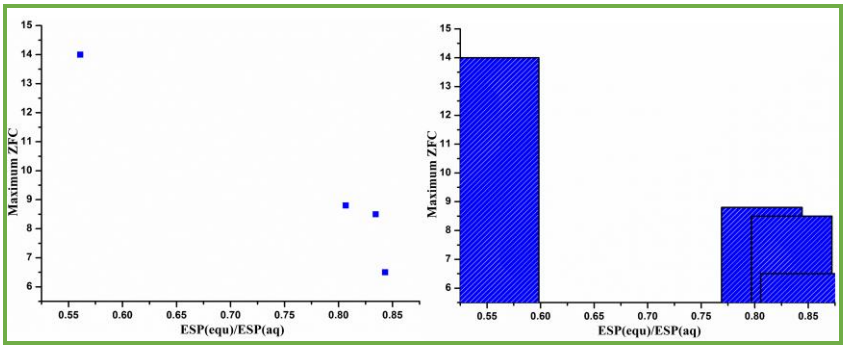

Figure S27. ESP(equ)/ESP(ax) *vs* maximum ZFC for complexes **1**, **2′** , **2** and **3**.

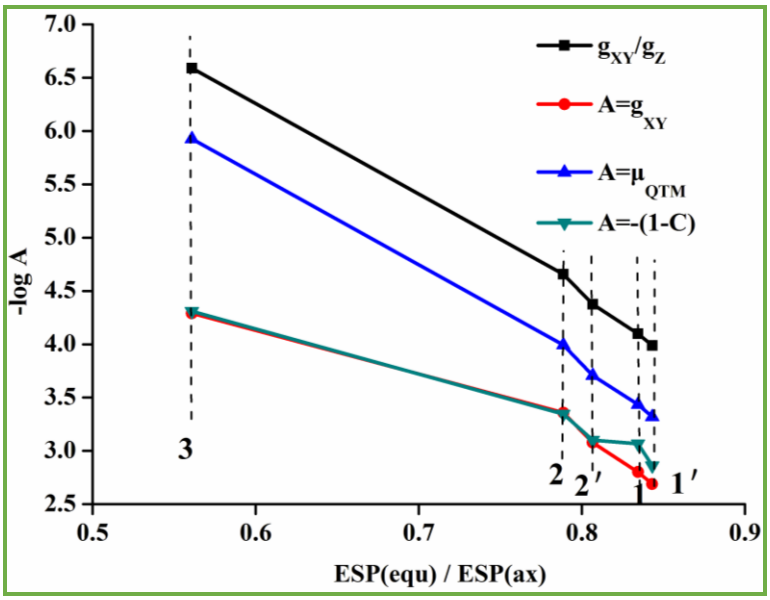

Figure S28. ESP(equ)/ESP(ax) *vs* –log A for complexes **1**, **1′** , **2**, **2′** and **3**.

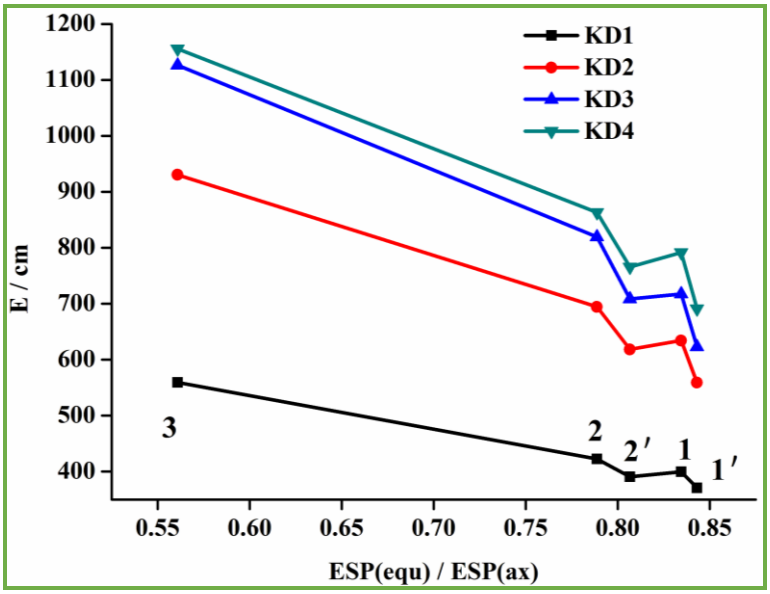

Figure S29. ESP(equ)/ESP(ax) *vs* E /cm for complexes **1**, **1′** , **2**, **2′** and **3**.

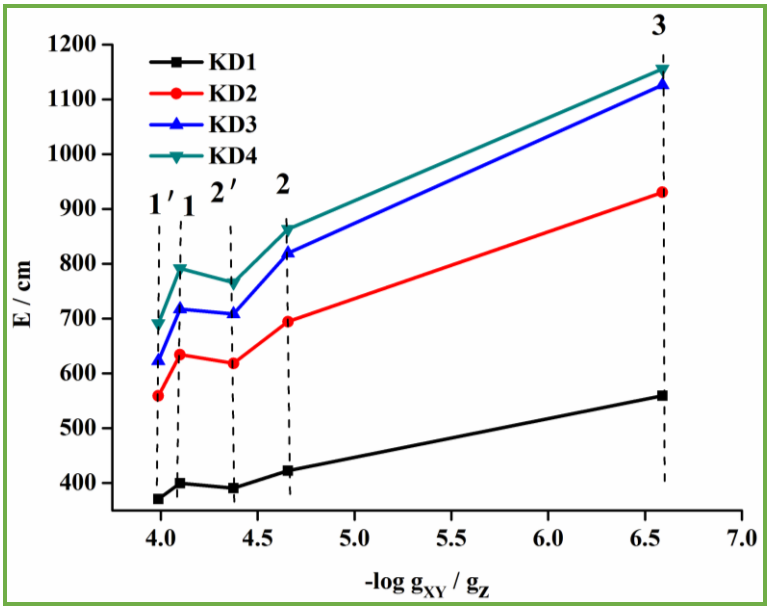

Figure S30. ESP(equ)/ESP(ax) *vs* E /cm for complexes **1**, **1′** , **2**, **2′** and **3**.

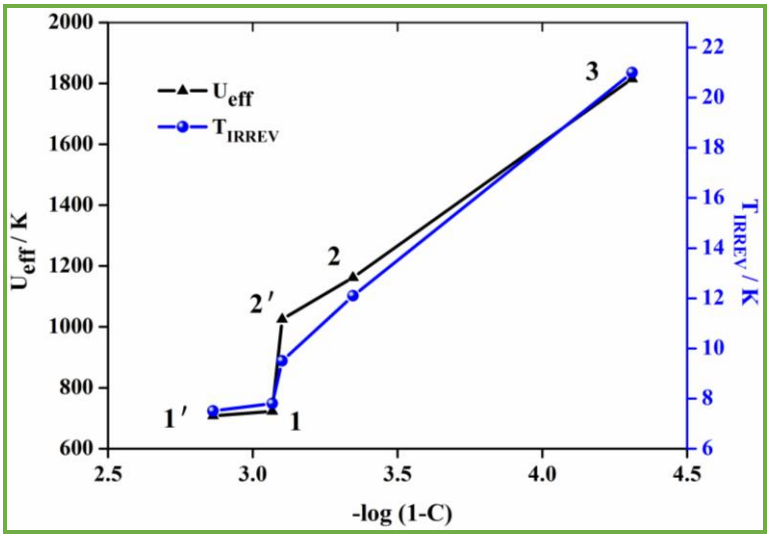

Figure S31. –log (1-C) *vs* U_{eff}, T_{IRREV} for complexes **1**, **1′** , **2**, **2′** and **3**.

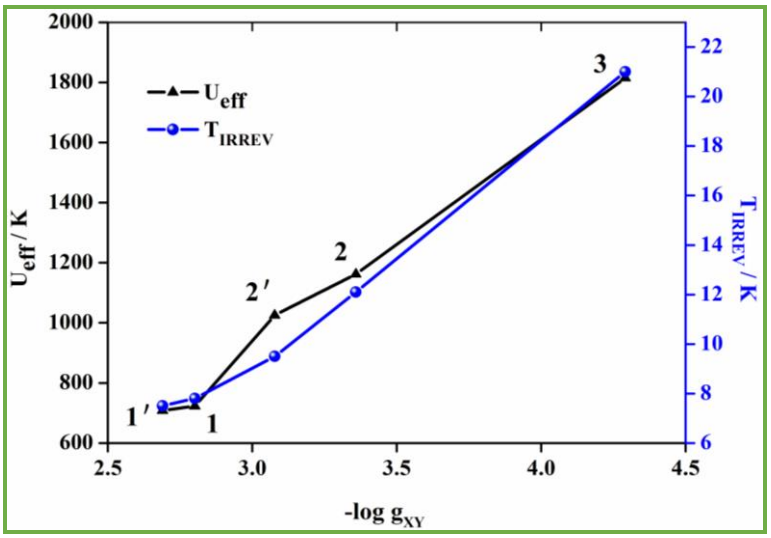

Figure S32. –log g_{XY} *vs* U_{eff}, T_{IRREV} for complexes **1**, **1′** , **2**, **2′** and **3**.